AFRL-VA-WP-TR-2006-3166

ANALYSIS AND SUPPORT INITIATIVE FOR STRUCTURAL TECHNOLOGY (ASIST)

Delivery Order 0045: Adaptive Structures - Based on Energy Design (ASBED)

Ramana Grandhi

Anteon Corporation
5100 Springfield Pike, Suite 509
Dayton, OH 45431

AUGUST 2005

Final Report for 26 July 2002 – 01 June 2005

AIR VEHICLES DIRECTORATE
AIR FORCE MATERIEL COMMAND
AIR FORCE RESEARCH LABORATORY
WRIGHT-PATTERSON AIR FORCE BASE, OH 45433-7542

NOTICE AND SIGNATURE PAGE

Using Government drawings, specifications, or other data included in this document for any purpose other than Government procurement does not in any way obligate the U.S. Government. The fact that the Government formulated or supplied the drawings, specifications, or other data does not license the holder or any other person or corporation; or convey any rights or permission to manufacture, use, or sell any patented invention that may relate to them.

This report is already in the public domain and was not reviewed by the Air Force Research Laboratory Wright Site (AFRL/WS) Public Affairs Office; it is available to the general public, including foreign nationals.

Copies may be obtained from the Defense Technical Information Center (DTIC) (http://www.dtic.mil).

AFRL-VA-WP-TR-2006-3166 HAS BEEN REVIEWED AND IS APPROVED FOR PUBLICATION IN ACCORDANCE WITH ASSIGNED DISTRIBUTION STATEMENT.

*//Signature//

EDWARD SCHOPLER
ASIST PROGRAM MANAGER

//Signature//

JAMES M. TUSS
Acting Chief, Advanced Structural Concepts Branch
Structures Division

//Signature//

DAVID M. PRATT, Ph.D.
Technical Advisor
Structures Division

This report is published in the interest of scientific and technical information exchange, and its publication does not constitute the Government's approval or disapproval of its ideas or findings.

*Disseminated copies will show "//Signature//" stamped or typed above the signature blocks.

REPORT DOCUMENTATION PAGE

Form Approved
OMB No. 0704-0188

1. REPORT DATE *(DD-MM-YY)*	2. REPORT TYPE	3. DATES COVERED *(From - To)*
August 2005	Final	07/26/2002 – 06/01/2005

4. TITLE AND SUBTITLE
ANALYSIS AND SUPPORT INITIATIVE FOR STRUCTURAL TECHNOLOGY (ASIST)
Delivery Order 0045: Adaptive Structures - Based on Energy Design (ASBED)

5a. CONTRACT NUMBER
F33615-98-D-3210-0045

5b. GRANT NUMBER

5c. PROGRAM ELEMENT NUMBER
62201F

6. AUTHOR(S)
Ramana Grandhi

5d. PROJECT NUMBER
A04Z

5e. TASK NUMBER

5f. WORK UNIT NUMBER
DN

7. PERFORMING ORGANIZATION NAME(S) AND ADDRESS(ES)

Anteon Corporation
5100 Springfield Pike, Suite 509
Dayton, OH 45431

8. PERFORMING ORGANIZATION REPORT NUMBER

9. SPONSORING/MONITORING AGENCY NAME(S) AND ADDRESS(ES)

Air Vehicles Directorate
Air Force Research Laboratory
Air Force Materiel Command
Wright-Patterson Air Force Base, OH 45433-7542

10. SPONSORING/MONITORING AGENCY ACRONYM(S)
AFRL-VA-WP

11. SPONSORING/MONITORING AGENCY REPORT NUMBER(S)
AFRL-VA-WP-TR-2006-3166

12. DISTRIBUTION/AVAILABILITY STATEMENT
Approved for public release; distribution is unlimited.

13. SUPPLEMENTARY NOTES
Report contains color. This report is already in the public domain and was not reviewed by the Air Force Research Laboratory Wright Site (AFRL/WS) Public Affairs Office.

14. ABSTRACT

The research in this study develops an analysis technique for mechanized solid-state actuators. The methodology's strength stems from the fact that it can be applied to a single solid-state actuator or an actuator that is coupled to a compliant mechanism (mechanized). The technique couples the actuator to any compliant mechanism and it takes into account interactions between the mechanized actuator and its load. Thus the methodology can be applied to a myriad of loaded systems. The analysis technique is rooted in thermodynamics and thus can be expanded to a wide range of systems (piezoelectric, electrohydraulic, electrostrictive, magnetostrictive, etc.). The methodology uses energy transfer as a medium to develop analytical relationships between input parameters and output parameters. Results of the technique are consistent with existing energy-based techniques and experimental data.

15. SUBJECT TERMS
Energy efficiency, Unloaded efficiency, Loaded efficiency, Solid-State Actuators

16. SECURITY CLASSIFICATION OF:			17. LIMITATION OF ABSTRACT:	18. NUMBER OF PAGES	19a. NAME OF RESPONSIBLE PERSON (Monitor)
a. REPORT	b. ABSTRACT	c. THIS PAGE			Ed Schopler
Unclassified	Unclassified	Unclassified	SAR	32	19b. TELEPHONE NUMBER *(Include Area Code)* N/A

Standard Form 298 (Rev. 8-98)
Prescribed by ANSI Std. Z39-18

FOREWORD

Many of the technical activities conducted in this project are conducted by Dr. James Joo, Research Assistant Professor of Wright State University, under contract F33615-98-D-3210, Delivery Order No. 45, "Adaptive Structures – Based on Energy Design (ASBED)" from AFRL/VAS.

Dr. Brian Sanders is the AFRL Program Manager (AFRL/VAS) and Dr. Ramana V. Grandhi is the principal investigator at Wright State University.

The report addresses the energy based design of morphing aircraft structures. The following two publications summarize the research accomplishments.

1. Energy Based Efficiency of Mechanical Solid-state Actuators (SPIE Conference)
2. Air Vehicle Control Using Multiple Control Surfaces (AIAA Conference)

Energy Based Efficiency of Mechanized Solid-State Actuators

Jinyong Joo[a], Brian Sanders[a], Gregory Washington[b], Jason Adams[b]

[a]Air Vehicles Directorate, Air Force Research Laboratory, Wright-Patterson AFB, OH 45433
[b]Department of Mechanical Engineering, Ohio State University

ABSTRACT

The research in this study develops an analysis technique for mechanized solid-state actuators. The methodology's strength stems from the fact that it can be applied to a single solid-state actuator or an actuator that is coupled to a compliant mechanism (mechanized). The technique couples the actuator to any compliant mechanism and it takes into account interactions between the mechanized actuator and its load. Thus the methodology can be applied to a myriad of loaded systems. The analysis technique is rooted in thermodynamics and thus can be expanded to a wide range of systems (piezoelectric, electrohydraulic, electrostrictive, magnetostrictive, etc.). The methodology uses energy transfer as a medium to develop analytical relationships between input parameters and output parameters. Results of the technique are consistent with existing energy-based techniques and experimental data.

Keywords: Energy efficiency, Unloaded efficiency, Loaded efficiency, Solid-State Actuators

1. INTRODUCTION

Air vehicles that are intended to function in multiple roles historically have compromised capabilities. Optimal performance for a multi-role aircraft throughout all phases of a mission profile would require significant geometric changes in the flight configuration. Current methodologies would yield cumbersome designs in which a few large actuators would move whole aerodynamic surfaces inefficiently. Recent efforts of the Active Aeroelastic Wing Technology Demonstration Program have shown that the integrated design of the wing structure and multiple control surface system will yield a lighter wing structure that meets all performance requirements. Highly integrated design of a distributed network of actuators embedded within a compliant structure that utilizes aeroservoelastic effects may yield a true multi-role air vehicle, capable of near optimal performance in all phases of a mission. To achieve this goal, we will use the energy as an optimization metric for the distribution of actuators and sensors.

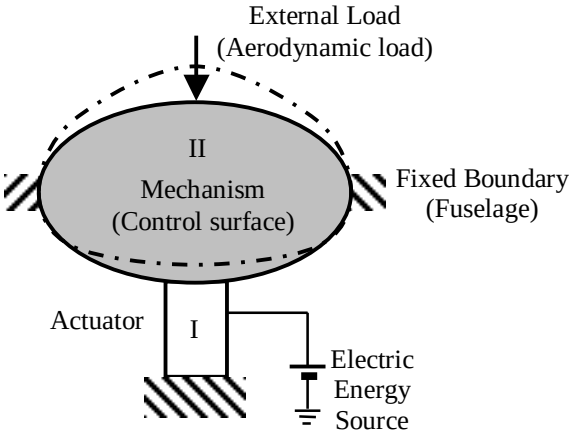

Figure 1: A simplified schematic of a mechanism shape change with an actuator under an external load

The utilization of energy as a behavior function has been employed in the synthesis of actuators [1,2,3], compliant mechanisms [4], airfoil shape [5], and tensegrity structures [6]. However, the implementation of this metric tends to be too specific to the problem description or under-estimates the actual energy requirements, to be applied to a general class of problems. Also, the energy relations within a system, such as stored energy, transferred energy, and total energy, are

Smart Structures and Materials 2003: Smart Structures and Integrated Systems,
Amr M. Baz, Editor, Proceedings of SPIE Vol. 5056 (2003) © 2003 SPIE · 0277-786X/03/$15.00

not clearly identified even though they are important factors to define energy efficiency of an actuated system. To better capture the internal energy relationships, and to provide a behavior function that can be utilized on a variety of problem descriptions, a new definition is desired for energy efficiency of (externally) unloaded and loaded systems with actuation.

The energy relations of a typical shape change system of an aircraft wing are investigated to develop a better understanding of the issues involved in the design of distributed actuation systems. We first develop expressions for the relationship of the energy required to deflect the control surface in a steady flow field, then proceed to define a new definition of (loaded and unloaded) energy efficiency and lastly verify the definition with simple experiments. A simplified schematic of the aerodynamic load and control surface with actuator system is shown in figure 1.

2. ENERGY EFFICIENCY

The unloaded efficiency is a unique value of the mechanism that depends on its structural stiffness and is not affected by external load. The loaded efficiency depends on the useful work of a mechanism, which is dependent upon the external load. This paper will concentrate on the definition of efficiency of a system with a constant external load.

2.1 Actuator (Electrical Energy to Mechanical Energy)

A solid-state actuator as shown in figure 2 is actuated with a driving voltage, V, with an unloaded output port. The unloaded efficiency is determined from the electric energy input into the actuator (figure 2a) and the force transferred from the actuator to the output port (figure 2b).

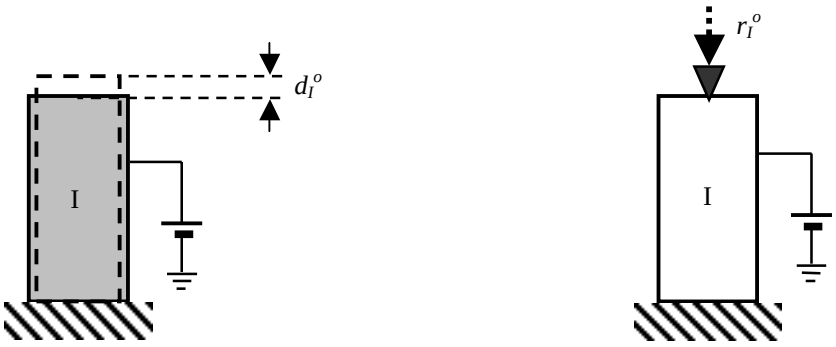

(a) (b)

Figure 2: Actuated System without Mechanism

The energy relations (force versus displacement diagrams) of the solid-state induced actuator are shown in figure 3. The energy input to the actuator is approximated by:

$$U_I^i = E_e = \Delta ABC = \frac{1}{2}QV = \frac{1}{2}CV^2 \tag{1}$$

where Q is a current charge and C is a capacitance of the actuator. The mechanical energy transferred to the output port (figure 2b) is determined from the displacement at the output port, d_I^o, and the block force, r_I^o, at the fixed output port:

$$U_I^{tr} = E_m = \Delta A'B'C' = \frac{1}{2}d_I^o r_I^o \tag{2}$$

The coupling coefficient that relates electrical energy input and mechanical energy output is defined by

$$k^2 = \frac{Mechanical\ energy(E_m)}{Electrical\ energy(E_e)} \tag{3}$$

The performance of a system is frequently represented by its energy efficiency that is defined by the ratio of the useful work to the input energy. However, the efficiency is not a suitable terminology to define an unloaded system because it is not performing any “useful” work. Instead, the definition of the unloaded efficiency is introduced for general cases

such as a shape change application without external loading. It is a unique value of a system and is always larger than the loaded efficiency which will be defined in the next section. Based on equations (1) - (3), the unloaded efficiency is defined as:

$$\eta_I^{unloaded} = \frac{Transferred\,energy\left(U_I^{tr}\right)}{Applied\,energy\left(U_I^{i}\right)} = \frac{\Delta A'B'C'}{\Delta ABC} = \frac{d_I^o r_I^o}{CV^2} = k^2 \tag{4}$$

The maximum unloaded efficiency is obtained when all the electrical energy (input energy) is converted to the mechanical energy (output energy) thus giving a maximum unloaded efficiency of 100 %.

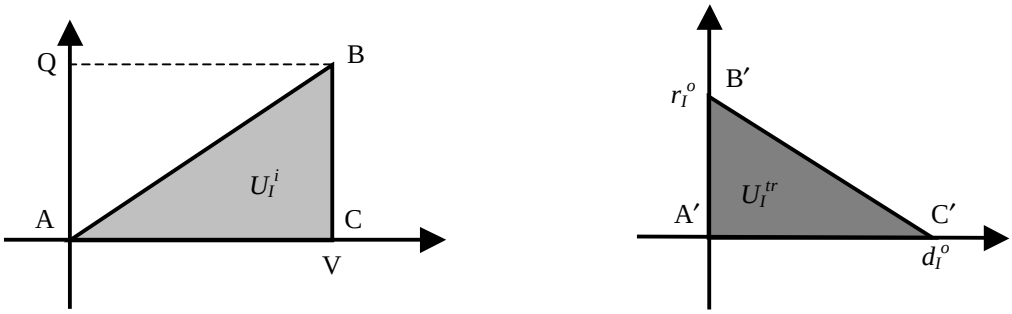

(a) At input port (b) At output port

Figure 3: Energy diagram measured at input and output port of a system

2.2 Actuator coupled with a mechanism (Actuator coupled with a linear structure)

In the previous section, the energy relation of a solid-state actuator is considered alone. The actuator is now attached at the input port of an arbitrary mechanism, as shown in figure 4, and an induced load is applied to the output port of the actuator which varies linearly with respect to the deformation ($f^i = k_{II}^i d_{II}^i$) of the body as described in figure 4. The energy output from the actuator to the input port of the body and the efficiency is determined from the stiffness of the mechanism, k_{II}^i , at the input port of mechanism.

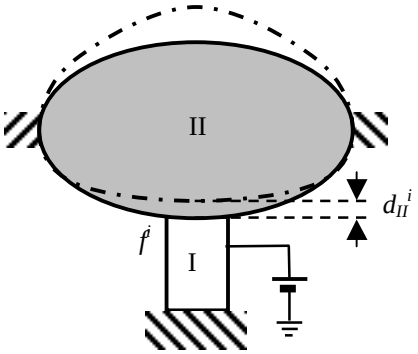

Figure 4: Actuator and unloaded mechanism

The energy relations (force versus displacement diagrams) at the input port of the mechanism are shown in figure 5. The energy input to the mechanism from an actuator is determined from the displacement of the input port, d_{II}^i, when the actuation force, f^i, is applied which is equal to or less than the actuator block force, r_I^o (figure 3b). The input energy from the actuator to the mechanism is equal to the transferred energy obtained from figure 2b (figure 5a).

$$U_I^{i'} = \Delta A'B'C' = \frac{1}{2} d_I^o r_I^o \tag{5}$$

Attaching an actuator to a mechanism changes the stiffness at the output port of the actuator; hence, the transferred energy to the mechanism needs to be measured based on figure 4 rather than figure 2. The transferred energy with the mechanism (the area of A′B′D′) is smaller than the energy without the mechanism (the area of A′B′C′) because the stiffness at the output port of the actuator is increased (the slope of the line B′D′). The mechanical energy transferred from the actuator, $U_I^{tr'}$, is determined from the displacement at the output port, d_{II}^i, and the reaction at the fixed output port, r_I^o (figure 4):

$$U_I^{tr'} = \Delta A'B'D' = \frac{1}{2} d_{II}^i r_I^o \tag{6}$$

Here, the slope of the line B′D′ and A′E′ represent the stiffness of the actuator at the output port and the stiffness at the input port of the mechanism, respectively.

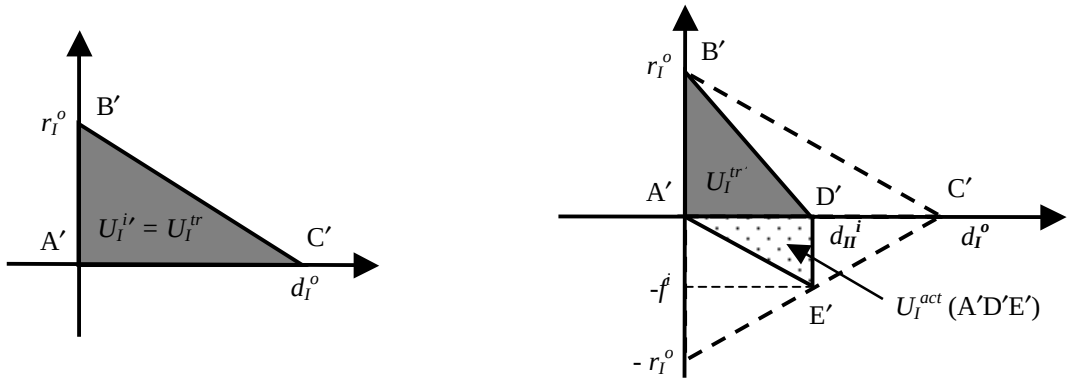

(a) Output energy of actuator (from figure 2b)

(b) Actual input work to the mechanism

Figure 5: Energy diagram measured at input and output port of a system

Given the assumption that energy is either transferred or stored, the stored mechanical energy inside of actuator is

$$\begin{aligned} U_I^{st'} &= \textit{Stored mechanical energy in the actuator} \\ &= \left(\Delta A'B'C' - \Delta A'B'D'\right) \end{aligned} \tag{7}$$

The total transferred mechanical energy from the actuator is

$$\begin{aligned} U_I^{tr'} &= \textit{Transferred mechanical energy from the actuator} \\ &= \Delta A'B'D' \end{aligned} \tag{8}$$

The total mechanical energy of the actuator which is the sum of the actuator's stored and transferred energy is defined geometrically as

$$U_I^{i'} = U_I^{st'} + U_I^{tr'} = \left(\Delta A'B'C' - \Delta A'B'D'\right) + \Delta A'B'D' = \Delta A'B'C' = \frac{1}{2} d_I^o r_I^o \tag{9}$$

The actual work done to the mechanism to move the input port in the amount of d_{II}^i is

$$U_I^{act} = \Delta A'E'D' = \frac{1}{2} f^i d_{II}^i \tag{10}$$

The energy relationships of the system consisting of an actuation force and a mechanism is identified by equations 6 through 10, and based on the diagram in figure 5, the unloaded efficiency of the actuator is defined using useful work U_I^{act} that is the stored energy in spring:

$$\begin{aligned} \eta_I^{loaded\,(spring)} &= \frac{Useful\,work\left(U_I^{act}\right)}{Applied\,energy\left(U_I^i\right)} = \frac{Transferred\,energy\left(U_I^{tr}\right)}{Applied\,energy\left(U_I^i\right)} \frac{Useful\,work\left(U_I^{act}\right)}{Input\,energy\left(U_I^{i'}\right)} \\ &= \frac{\Delta A'B'C'}{\Delta ABC} \frac{\Delta A'E'D'}{\Delta A'B'C'} = k^2 \frac{d_{II}^i f^i}{d_I^o r_I^o} \left(where\ f^i = k_{II}^i d_{II}{}^i\right) \end{aligned} \tag{11}$$

The useful work is determined according to the stiffness of the mechanism; If the stiffness of k_{II}^{i} is very small (k_{II}^{i} << 1), the useful work will be close to zero since the spring force, f^{i}, is close to zero. In the opposite case if (k_{II}^{i} >>1), the useful work still is close to zero because d_{II}^{i} is close to zero. The area of the useful work becomes maximum when the stiffness, k_{II}^{i} (the slope of A′E′), is same as the slope of B′C′. At that moment, the input force, f^{i}, is equal to half of the transferred force, r_{I}^{o}, and the useful work, U_{I}^{act} (area A′D′E′), is half of the maximum transferred energy, $U_{I}^{tr'}$ (area A′B′D′), and this is a quarter of the maximum transferred/input energy (the area of A′B′C′), i.e., 25% when k^2 is equal to one.

2.3 Mechanism (Mechanism without external force)

For the following two sections an arbitrary mechanism is focused with a constant actuation force. A mechanism as shown in figure 6 has an actuation at its input port and an unloaded output port. The unloaded efficiency is determined from the energy input to the mechanism from an actuator at the input port (figure 6a) and the force transferred from the actuator to the output port (figure 6b). Note we assume that the force r_{II}^{o} is the force that would be measured if the mechanism were constrained and not allowed to move. Since the mechanism is not loaded this force is fictitious (and is represented by a dotted line).

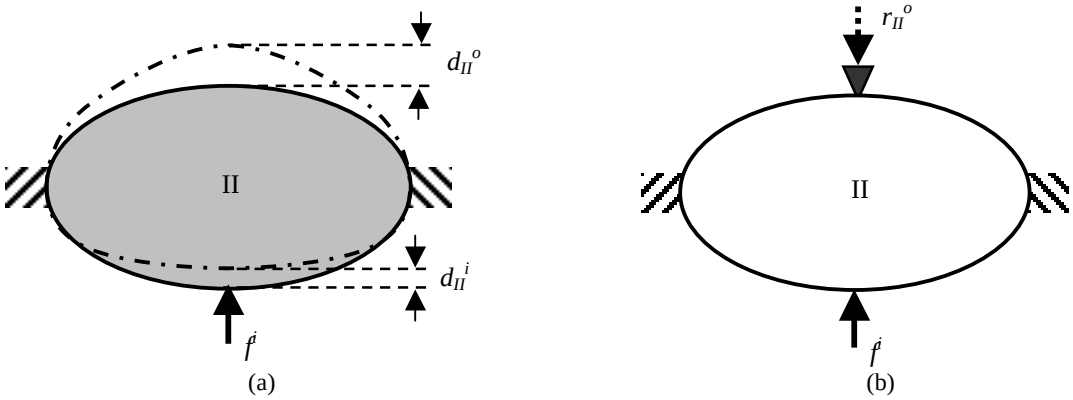

Figure 6: Unloaded Actuated mechanism

The energy relations (force versus displacement diagrams) for the input port and output port are shown in figure 7. The energy input to the mechanism from an actuator at the input port (figure 6a) is determined from the displacement of the input port, d_{II}^{i}, and the actuation force, f^{i}:

$$U_{II}^{i} = \Delta A'E'D' = \frac{1}{2} d_{II}^{i} f^{i} = U_{I}^{act} \tag{12}$$

The mechanical energy transferred from the actuator to the output port (figure 6b) is determined from the displacement at the output port, d_{II}^{o}, and the reaction at the fixed output port, r_{II}^{o}:

$$U_{II}^{tr} = \Delta FGH = \frac{1}{2} d_{II}^{o} r_{II}^{o} \tag{13}$$

Given the assumption that energy is either transferred or stored, the stored energy inside of mechanism is

$$U_{II}^{st} = \textit{Stored energy in the body} = \left(\Delta A'E'D' - \Delta FGH\right) = \frac{1}{2} d_{II}^{i} f^{i} - \frac{1}{2} d_{II}^{o} r_{II}^{o} \tag{14}$$

The total energy is the sum of the stored energy and the transferred energy:

$$U_{II}^{i} = U_{II}^{st} + U_{II}^{tr} = \left(\Delta A'E'D' - \Delta FGH\right) + \Delta FGH = \Delta A'E'D' = \frac{1}{2} d_{II}^{i} f^{i} \tag{15}$$

Based on equations 12 to 15 and based on the diagram in figure 7, the unloaded efficiency is defined as:

$$\eta_{II}^{unloaded} = \frac{Transferred\,energy\left(U_{II}^{tr}\right)}{Appliedenergy\left(U_{II}^{i}\right)} = \frac{\Delta FGH}{\Delta A'E'D'} = \frac{d_{II}^{o} r_{II}^{o}}{d_{II}^{i} f^{i}} \tag{16}$$

The maximum unloaded efficiency is obtained when the input energy is transferred to the output port without storing energy ($U_{II}^{i} = U_{II}^{tr}$) inside the mechanism. An example of this is an extremely stiff body that connects the input and output port with a very flexible (hinge like) link that connects the body and ground. The transferred energy (U_{II}^{tr}) is at its maximum, which translates to a maximum unloaded efficiency of 100 %.

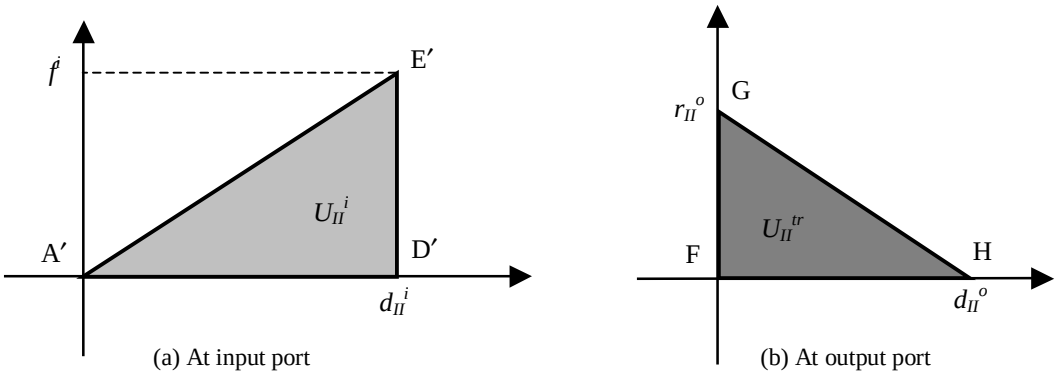

Figure 7: Energy diagram measured at input and output port of a system

2.4 Mechanism with an external load (Mechanism with a constant external force)

An arbitrary mechanism, as shown in figure 8, with an actuation input port and an externally loaded output port is considered. The loaded efficiency is determined from the energy that is input to the mechanism from an external load at the output port (figure 8a), the force transferred from the external load to the input port (figure 8b), the energy input to the mechanism from an actuator at the mechanism's input port (figure 8c), and the force transferred from the actuator to the output port (figure 8d). The simultaneous combination of forces and displacements at the input and output ports of the externally loaded, actuated mechanism are shown in figure 8e.

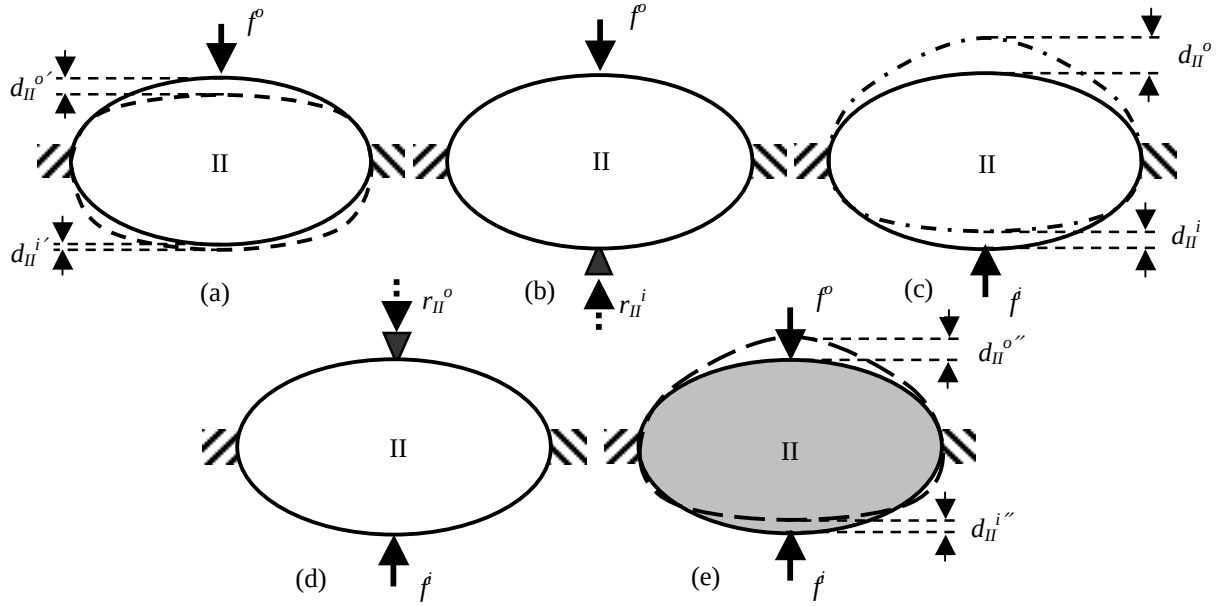

Figure 8: Loaded actuated mechanism with an external load

The energy relations (force versus displacement diagrams) for the input port and output port are shown in figure 9. The energy input to the mechanism from an external load, f^o, at the output port (figure 8a) is determined from the displacement of the output port, $d_{II}^{o'}$, and the external load, f^o:

$$U_{II}^{o} = \Delta FJF' = \frac{1}{2} d_{II}^{o'} f^o \tag{17}$$

Here, the material stiffness at the output port (slope of the line FJ) is assumed to match with the slope of the line GH for a linear system. The energy transferred from an external load, f^o, to the input port (figure 8b) is determined from the displacement of the input port, d_{II}^{i}, and the reaction force at the fixed input port, r_{II}^{i}:

$$U_{tr}^{i} = \Delta AIA'' = \frac{1}{2} d_{II}^{i} r_{II}^{i} \tag{18}$$

The energy input to the mechanism from an actuator at the input port (figure 8c) is determined from the displacement of the input port, d_{II}^{i}, when the actuation force, f^i, is applied without external loading, f^o:

$$U_{II}^{i'} = \Delta A'E'D' = \Delta A''E''D'' = \frac{1}{2} d_{II}^{i} f^i = U_{II}^{i} \tag{19}$$

The energy transferred from the actuator to the output port (figure 8d) is determined from the displacement at the output port, d_{II}^{o}, and the reaction at the fixed output port, r_{II}^{o}:

$$U_{tr}^{o} = \Delta FGH = \Delta F'G'H' = \frac{1}{2} d_{II}^{o} r_{II}^{o} \tag{20}$$

To guarantee positive output displacement, the transferred energy from the actuator must be greater than the energy input to the mechanism from an external load, f^o, at the output port:

$$U_{tr}^{o} > U_{II}^{o} \tag{21}$$

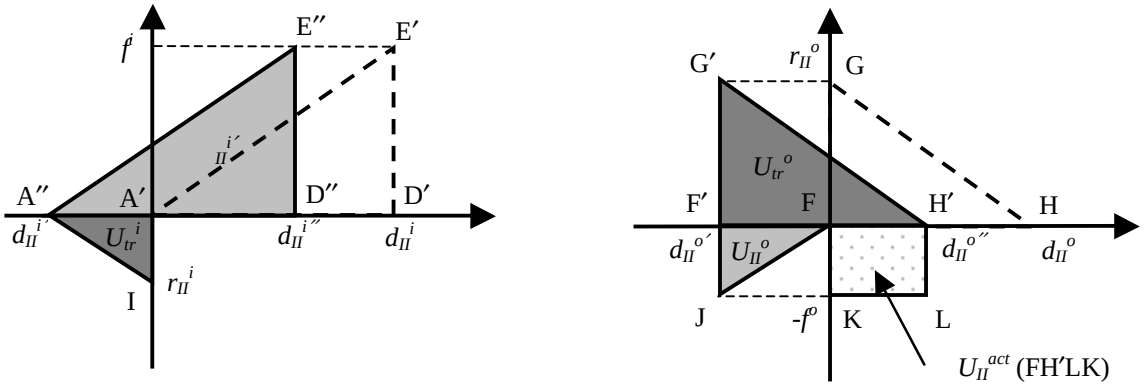

(a) Input port (b) Output port

Figure 9: Energy diagram measured at input and output port of a system

The stored energy inside of the mechanism from the actuation energy is

$$\begin{aligned} U_{II}^{st'} &= Stored\ \ energy\ \ by\ \ actuation \\ &= \left(\Delta A'E'D' - \Delta F'G'H'\right) \end{aligned} \tag{22}$$

The total transferred energy by the actuator to the output port is

$$\begin{aligned} U_{II}^{tr'} &= Transferred\ energy\ by\ input \\ &= \Delta F'G'H' \end{aligned} \tag{23}$$

The total input energy from the actuation is

$$
\begin{aligned}
U_{II}^{i'} &= U_{II}^{i} = U_{II}^{st'} + U_{II}^{tr'} \\
&= \left(\Delta A'E'D' - \Delta F'G'H'\right) + \Delta F'G'H' \\
&= \Delta A'E'D'
\end{aligned} \tag{24}
$$

The energy relationships (shown in figure 9) for the system experiencing an actuation force and external loading is identified by equations 17 through 24. The loaded efficiency of the system is defined as:

$$
\eta_{II}^{loaded} = \frac{\textit{Useful work } \left(U_{II}^{act}\right)}{\textit{Input energy } \left(U_{II}^{i'}\right)} = \frac{FH'LK}{\Delta A'E'D' (= \Delta A''E''D'')} = \frac{d_{II}^{o''} f^{o}}{\frac{1}{2} d_{II}^{i} f^{i}} \tag{25}
$$

The loaded efficiency depends on the external load because the useful work is determined according to the external force; If the external load is large, the output displacement is small, then, the output work is small due to the small displacement. If the external load is small, the output displacement is large but it is not doing much work because the force is small. Therefore, the maximum efficiency is found where the external load and displacement are unbiased. The maximum loaded efficiency is obtained when the input energy is transferred to the output port without loosing energy ($U^{i} = U_{tr}^{o}$) and the external load, f^{o}, is equal to half of the transferred force, r^{o}, when output port is fixed. When this occurs it can be shown that the useful work (U_{II}^{act}) is at its maximum, which translates to a loaded efficiency of 50 %.

For certainactuators such stack PZT's, the maximum efficiency may be a value other than half of the transferred force, r_{II}^{o}. For small forces, the stiffness of piezoceramic depends on the spring constant which relates the influence of the external load to the dimensional change of the material. For larger forces, it is necessary to include an additional term describing the polarization of PZT ceramic, which is affected by both the drive voltage and external forces. This leads to the fact that the slope of G′H′ of actuators is not necessarily equivalent to the stiffness of PZT ceramic itself. When the stiffness of the piezoceramic (the slope of the line FJ) is smaller than the slope of G′H′, the maximum efficiency may be found at an external load, f^{o}, that is less than the half of the transferred force, r_{II}^{o}, and vice versa (Figure 10a and 10b). In this paper, the stiffness is assumed to be equal to the spring constant of the material regardless the range of driving voltage or force to simplify the problem. Also, note that the rest of energy is used to deform the structure and stored in the body as a strain energy form. This energy will be used to recover the actuator back to its original undeformed shape when the electrical voltage and external load are removed, hence, this energy is not exactly lost. However, this energy is considered as a loss for now because it is not transferred to the output port and used to perform work.

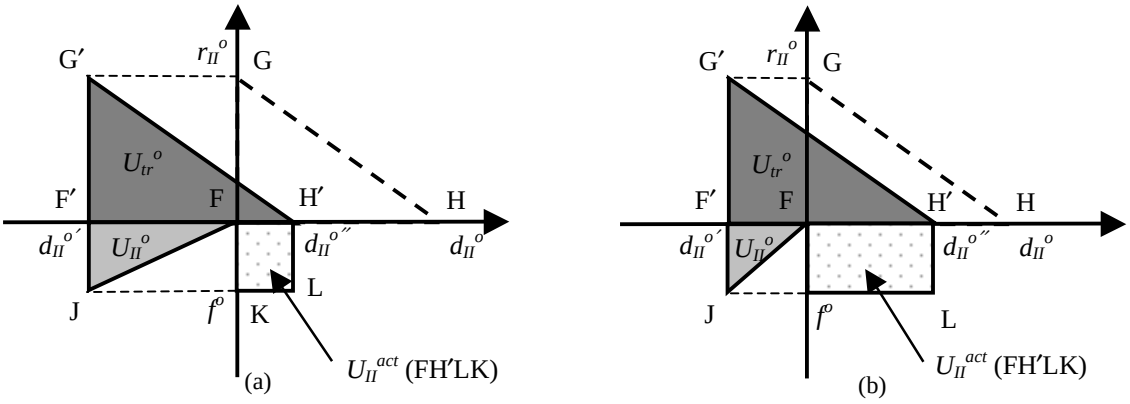

Figure 10: Energy diagram for PZT actuators

2.5 Total efficiency

The loaded efficiency of the system in figure 1 is now defined as

$$\eta_{I\to II}^{loaded} = \frac{Useful\ work\ \left(U_{II}^{act}\right)}{Input\ energy\ \left(U_I^i\right)} = \frac{FH'LK}{\Delta ABC} = \frac{d_{II}^{o''} f^o}{\frac{1}{2}CV^2} \tag{26}$$

This can be expressed as

$$\begin{aligned}\eta_{I\to II}^{loaded} &= \frac{Useful\ work\ \left(U_{II}^{act}\right)}{Input\ energy\ \left(U_I^i\right)} \\ &= \left(\frac{U_I^{act}}{U_I^i}\right)\left(\frac{U_{II}^{act}}{U_{II}^{i'}}\right) \quad \left(\because U_I^{act} = U_{II}^{i'}\right) \\ &= \eta_I^{loaded(spring)}\eta_{II}^{loaded(const)}\end{aligned} \tag{27}$$

The total efficiency is the multiplication of the loaded efficiency of the actuator and mechanism. Note that the loaded efficiency is used for the total efficiency calculation rather than unloaded efficiency. When the actuator and mechanism are designed separately and combined together, the interactions between actuator and mechanism need to be considered in advance to calculate the total efficiency using the equation 27. Knowing that the maximum of the spring loaded efficiency of the actuator and maximum of the constant loaded efficiency of the mechanism are 25% and 50% respectively, the maximum efficiency of the simplified adaptive structure model in figure 1 is

$$\left(\eta_{I\to II}^{loaded}\right)_{\max} = \left(\eta_I^{loaded(spring)}\right)_{\max}\left(\eta_{II}^{loaded(const)}\right)_{\max} = (25\%)(50\%) = 12.5\% \tag{28}$$

3. EXAMPLES

In this paper the unloaded and spring-loaded efficiency of an actuator is calculated. We choose a high displacement piezomotor actuator (Part # 300HD) manufactured by Kinetic Ceramics for this test. The unloaded efficiency is obtained based on data provided by the vendor and the force-displacement plot of the actuator is obtained using springs with three different stiffness.

The maximum electrical input energy is calculated based on equation 1:

$$U_I^i = E_e = \Delta ABC = \frac{1}{2}QV = \frac{1}{2}CV^2 = \frac{1}{2}\left(0.56\times10^{-6}\ \text{F}\right)\left(1000\ \text{V}\right)^2 = 0.28\ \text{J}$$

The maximum mechanical output based on equation 2:

$$U_I^{tr} = E_m = \Delta A'B'C' = \frac{1}{2}d_I^o r_I^o = \frac{1}{2}\left(300\times10^{-6}\ \text{m}\right)(445\ \text{N}) = 0.0667\ \text{J}$$

Therefore, the maximum unloaded efficiency of the actuator based on vendor information based on equation 4:

$$\eta_I^{unloaded} = \frac{Transferred\ energy\left(U_I^{tr}\right)}{Applied\ energy\left(U_I^i\right)} = \frac{0.0667}{0.28} = 0.2382 \approx 24\%$$

The maximum driving voltage for the loaded efficiency test was 600V and the displacement is measured at a frequency of 0.005 (Hz) in order to make the results quasistatic. Three different springs are used to get the force displacement curve and they are linearly fit to the three data points. The input energy for this test is

$$U_I^i = E_e = \Delta ABC = \frac{1}{2}QV = \frac{1}{2}CV^2 = \frac{1}{2}\left(0.56\times10^{-6}\ \text{F}\right)\left(600\ \text{V}\right)^2 = 0.10\ \text{J}$$

The maximum force and free displacement from the curve are 105 (N) and 0.107 (mm), respectively. Based on these numbers the transferred energy when actuator is driven at 600 (V) is 0.0056 (J), which is about 23% of the energy its supposed to be (0.5 * 445N*0.6 × 300μm*0.6 = 0.024 J). More experiments are required to figure out the reason but we will focus on trends of useful work as stiffness changes in this paper. The useful work to deform each spring based on equation 10 with test data:

$$\left(U_I^{act}\right)_{K=320} = \frac{1}{2}f^i d_{II}^i = \frac{1}{2}(25.3\text{N})(0.0789\text{mm}) = 0.0010\text{J}$$

$$\left(U_I^{act}\right)_{K=600} = 0.0014\,\text{J} \quad \text{and} \quad \left(U_I^{act}\right)_{K=1285} = 0.0013\,\text{J}$$

Therefore, the spring-loaded efficiencies of the actuator based on equation 11:

$$\left(\eta_I^{loaded}\right)_{K=320} = \frac{U_I^{act}}{U_I^i} = \frac{0.0010\text{J}}{0.10\text{J}} = 0.01\,(1\%)$$

$$\left(\eta_I^{loaded}\right)_{K=600} = 0.014\,(1.4\%) \quad \text{and} \quad \left(\eta_I^{loaded}\right)_{K=1285} = 0.013\,(1.3\%)$$

Table 1: Specification for 300HD

High displacement piezomotor actuator (300HD)			
Max. voltage	Max. displacement	Capacitance	Max. Force
1000 V	300 μm @ 1000 V	0.56 μF	445 N

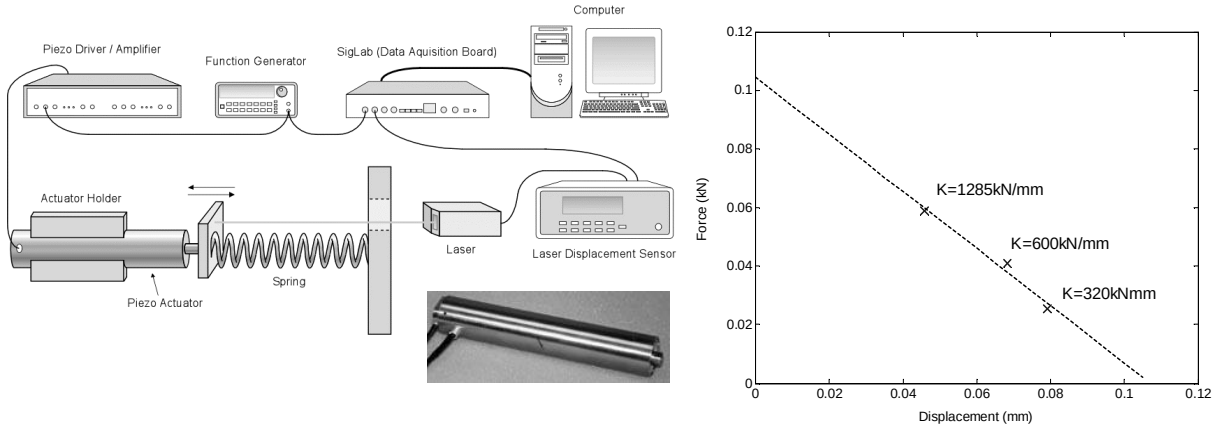

Figure 11: Experiment setup and results plot

4. SUMMARY

The unloaded and loaded efficiencies of uncoupled and coupled actuator-mechanism systems are defined for a general class of problems. The maximum efficiencies of the uncoupled actuator or mechanism are 25% for the spring-loaded case and 50% when a constant force loaded case with a linear force-displacement relation, static loading conditions, and a piezoelectric coupling coefficient, k^2, of one are assumed. Experimental validation of this methodology is described using a PZT motor and an external spring, which models the spring loaded actuator. The efficiency found in the experiment is on the order of 1.5%. At this time it is thought that the discrepancy is due to the nonlinear response of the force-displacement curve of the actuator, which is a result of the internal displacement magnification mechanism. However, further investigation is required to valid this observation. Also the maximum efficiency of the simple adaptive structure model under a constant external load is derived as the product of maximum loaded efficiency of each component. It is shown that the maximum efficiency is 12.5%.

5. ACKNOWLEDGEMENT

The authors would like to acknowledge the support of the Air Force Office of Scientific Research, Structural Mechanics Program.

REFERENCES

1. Giurgiutiu, V and Rogers, C.A. "Dynamic Power and Energy Capabilities of Commercially-Available Electro-Active Induced-Strain Actuators," *Journal of Intelligent Material Systems and Structures*, **7**: 656-667, 1996.
2. Prechtl, E. F. and Hall, S. R. "Design of a High Efficiency, Large Stroke, Electromechanical Actuator," *Smart Material and Structures*, **8**: 13-30, 1999.

3. Leo, D. " Energy Analysis of Piezoelectric-Actuated Structures Driven by Linear Amplifiers", *ASME Adaptive Structures and Material Systems*, AD-87: 1-10, 1999.
4. Hetrick, J. A. and Kota, S. " Size and Shape Optimization of Compliant Mechanisms: An Efficiency Formulation," *1998 ASME Design Engineering Technical Conference*, DETC98/MECH-5943, 1998.
5. Prock, B. C., Weisshaar, T. A., and Crossley, W. A., " Morphing Airfoil Shape Change Optimization with Minimum Actuator Energy As An Objective", *9th AIAA/ISSMO Symposium on Multidisciplinary Analysis and Optimization*, AIAA 2002-5401, 2002.
6. Skelton, R. E., "An Introduction To The Mechanics of Tensegrity Structures", Downloaded from http://www.mae.ucsd.edu/research/reskelton/

Air Vehicle Control Using Multiple Control Surfaces

Brian Sanders[†1], Greg Reich[‡] , Jinyong Joo[§§], Frank Eastep[§§]
Air Force Research Laboratory, Wright-Patterson AFB, Ohio 45433

This project is investigating the use of wide span, smoothly varying control surfaces placed on the leading and trailing edges of a wing to control cruise and maneuver performance of a representative combat unmanned vehicle. The purpose of the research is to understand the desired mechanical characteristics as well as the optimum deflection distribution in the spanwise and chordwise directions. In particular we are looking for the shapes of the control surfaces such that roll, pitch, and yaw control are maximized while the necessary input energy (actuator) is minimized during maneuvering phase of a mission. We are also looking at using the same set of control surfaces to minimize the induced drag during the cruise portion of the flight. Several objective functions where investigated to gain insight into minimizing the actuator requirements. The optimization schemes satisfied equilibrium conditions. Results indicate that multiple control surfaces have the potential to offer greater flexibility to the aircraft designer for controlling a vehicle over the entire flight spectrum, and that the distribution is strongly dependent on the selected objective function.

Nomenclature

b	Span (ft)
c	Chord (ft)
S	Wing area (ft^2)
C_{L_α}	Lift coefficient due to angle of attack
C_{L_p}	Roll moment coefficient due to roll rate
$C_{L_{\delta_{cs}}}$	Roll moment coefficient due to control surface deflection
L	Lift (lbs)
M_h	Hinge moment (ft-lbs)
p	Roll rate (deg/sec)
U_∞	Free stream velocity (ft/sec)
ρ_∞	Free stream density (slugs/ft^3)
q	Dynamic pressure (psf)
α	Angle of attack (degrees)
δ	Control surface deflection (degrees)

I. Introduction

Since the late 1970's researchers have investigated a few options for controlling an aircraft using multiple control surfaces in a coordinated fashion. The Mission Adaptive Wing[1] (MAW) program was perhaps the first program to demonstrate multiple control surfaces that where smoothly contoured in the chordwise direction. In this program the trailing edge was segmented into three discrete segments. This enabled a spanwise distribution of control surfaces for use during cruise and maneuver segments of flight. The vehicle was also configured with a single, smoothly contoured leading edge control surface that ran the entire semispan of the wing. The MAW program flight program demonstrated large improvements in the performance of a supersonic fighter in the transonic regime.

1

[†]AFRL/VASD, email:brian.sanders@wpafb.af.mil, AIAA Associate Fellow
[‡]AFRL/VASA, email: gregory.reich@wpafb.af.mil, AIAA Senior Member
[§]AFRL/VASA: email: jinyong.joo@wpafb.af.mil
[§§] NRC, email: franklin.eastep@wpafb.af.mil, AIAA Fellow

Another exciting program using multiple surfaces is the Active Aeroelastic Wing[2] (AAW) program. AAW technology takes advantage of the energy in the airstream to control the spanwise variation of twist on a wing. This is currently accomplished using four control surfaces on each semispan of the wing – two on the leading edge and two on the trailing edge. The AAW program has demonstrated in wing tunnel experiments that smaller control surface deflections are possible while still maintaining high control power. This translates into lower actuator power required and less wing weight.

Improvements in actuator technology have lead to more innovations in control surface design. One such demonstration of this is the Smart Wing program[3]. In this program, piezoelectric based ultrasonic motors were integrated into a novel control surface design. The trailing edge of a representative unmanned combat air vehicle was configured with 10 of these control surfaces. This technology enabled a smooth variation in both the chordwise and spanwise directions while meeting deflections and deflection rates required for control of the UCAV.

The Smart Wing program primarily focused on the mechanical aspects of the technology. We still need to explore the design space before we understand how to apply it. The main objective of the current research is to further explore the use of these control surfaces using some of the lessons learned from the MAW and AAW programs. This paper will deal specifically with the roll and drag performance of an air vehicle enabled with the Smart Wing Technology.

II. Analysis Tools and Model Configuration

Two optimization problems are addressed in this paper. The first is for roll control and can be expressed as

$$\min \quad f(y) \tag{1}$$

Subject to:

$$C_{L_\alpha} \frac{pb}{2U_\infty} + \sum C_{L_{\delta_i}} \delta_i = 0 \tag{2a}$$

$$ay^2 + by + c = z \tag{2b}$$

$$\delta_{\max} \le \delta_i \le \delta_{\min} \tag{2c}$$

Equation (2) is the trim condition that satisfies equilibrium for a steady roll rate. Equation three is a constraint that forces the distribution of displacements in the spanwise direction to assume a second order shape, and equation (4) represents the deflection limit for any control surface. Several minimization functions ~~(f(y))~~ have been explored. The first is the minimization of displacements, which can be expressed as

$$f(y) = \sum_{i=1}^{n} \delta_i^2 \tag{3a}$$

The second is the minimization of the hinge moment

$$f(y) = \sum_{i=1}^{n} M_i^2 \tag{3b}$$

The third is minimizing work, which was looked at two ways as shown below

$$f(y) = \sum_{i=1}^{n} W_i^2 \tag{3c}$$

$$f(y) = \sum_{i=1}^{n} W_i \tag{3d}$$

The second optimization problem is drag minimization for a cruise or loiter condition, which can be expressed as

$$\min \quad \sum \left(\left\{ L_{elliptic} \right\} - \left\{ L_{computed} \right\} \right)^2 \tag{4}$$

Subject to:

$$qS\left(C_{L_\alpha}\alpha + \sum C_{l_{\delta_i}}\delta_i\right) = W \tag{5a}$$

$$ay^2 + by + c = z \tag{5b}$$

$$\delta_{\max} \le \delta_i \le \delta_{\min} \tag{5c}$$

For this situation, the objective function is the difference between an elliptic lift distribution for a rigid wing and that distribution that would occur on a flexible wing. This is accomplished using the multiple control surfaces to redistribute the aerodynamic loads. The constraint simply describes the flight vehicle equilibrium in level, unaccelerated flight.

The semispan platform selected for this investigation is shown in Figure 1. This is a flying wing configuration and is considered representative of typical UCAV. Since we are primarily interested in aeroelastic effects, we selected a simple 11 node, beam-rod representation of the wing structure. It is located at 40% of the chord. The distribution of structural properties is given in Fig. 2. The fuselage component is assumed to be rigid. The control surfaces compose 25% of the chord on leading and trailing edge of the wing surface. The dash line in Figure 1 shows the actual location of the wing tip. The aerodynamic grid was modified as shown in the figure to allow for a better panel representation in the streamwise direction in this location.

Parameters selected for the analysis where those that are considered typical of a vehicle conducting a hunter-killer mission. For example, the vehicle may cruise and loiter at a moderate altitude and than dash and maneuver at a low altitude. For this paper, the swept wing configuration (Fig 1a) is investigated for a sea level dash at a Mach number of 0.8 . The necessary aerodynamic coefficients were found using the Automated Structural Optimization System[4] (ASTROS). ASTROS is a finite element based program with integrated aerodynamic panel methods. The optimization problem was then solved using MATLAB since ASTROS does not currently solve the type of problem we are investigating.

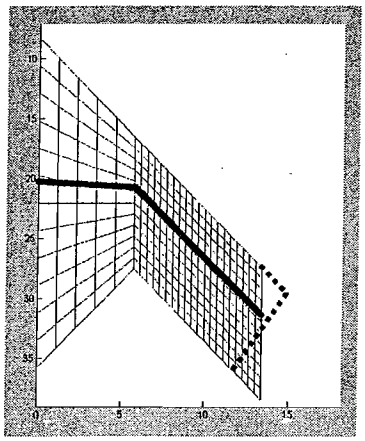

Figure 1 Representative UCAV Aerodynamic Planform

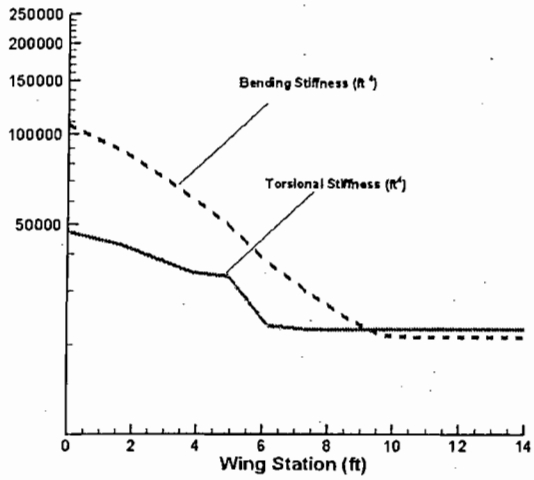

Figure 2 Wing Bending and Torsion Stiffness Distribution

III. Results and Discussion

Roll Performance

Before proceeding into multiple surface configurations on the representative flight vehicle, we investigate the optimization scheme on a flexible straight wing with only one leading and one trailing edge control surface. The wing has a semispan of 20 feet and a chord of 6 feet. Each control surface has a 10 foot span and a 1.5 foot chord. The structural properties can be found in Ref 5. Figure 3 shows the control surface displacements as a function of the dynamic pressure computed using the optimization routine described above. Figure 3a (left side) shows the displacements resulting from minimizing the displacements while Figure 3b (right side) shows the displacements resulting from trying to minimize hinge moment.

The result obtained here for the minimum displacement is similar to those found in Ref 5. The trend appears to be dominated by the effectiveness of the trailing edge control surface. For example, as the dynamic pressure increases and the roll moment coefficient of the trailing edge reduces, so does the amount of deflection that the optimization scheme produces for this control surface. At the point where the control surface reverses, approximately 300 psf, the trailing edge control surface has a zero deflection and all of the roll authority comes from deflecting the leading edge. The magnitude of the control surface displacement resulting from a minimization of the hinge moments is on the same order. However, the scheme continues to utilize the trailing edge surface even when it is not particularity effect. This is a result of the magnitude of the overall hinge moment which is discussed next. Similar plots are presented in the talk related to the optimization based on work.

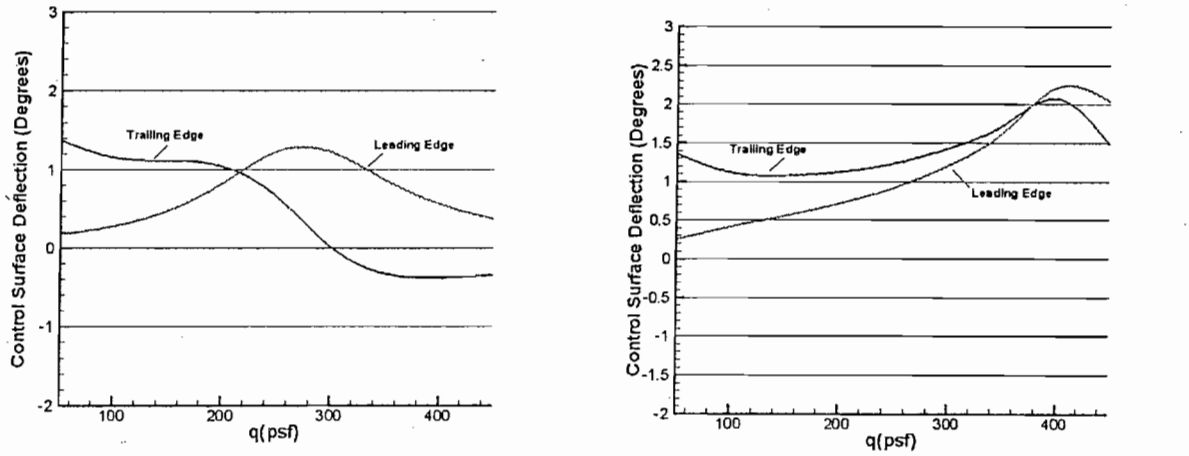

Figure 3 Control Surface Deflections for (a) Minimizing Displacement, (b) Minimizing Hinge Moment

Figure 4 shows the trend in the hinge moments for each of the two cases discussed above. It can be observed that the peak hinge moment occurs for the case when we were trying to minimize the displacement. It is interesting to observe the trend in the hinge moment for the leading edge control surface when the hinge moment is trying to be minimized. The hinge moment is very small over most of the dynamic pressure regime investigated. This is most likely the result of the low aerodynamic force on the leading edge in these conditions, which results from the nose down pitching moment induced when the trailing edge is deflected. More investigation into the aerodynamic pressure profiles needs to be performed to verify this observation.

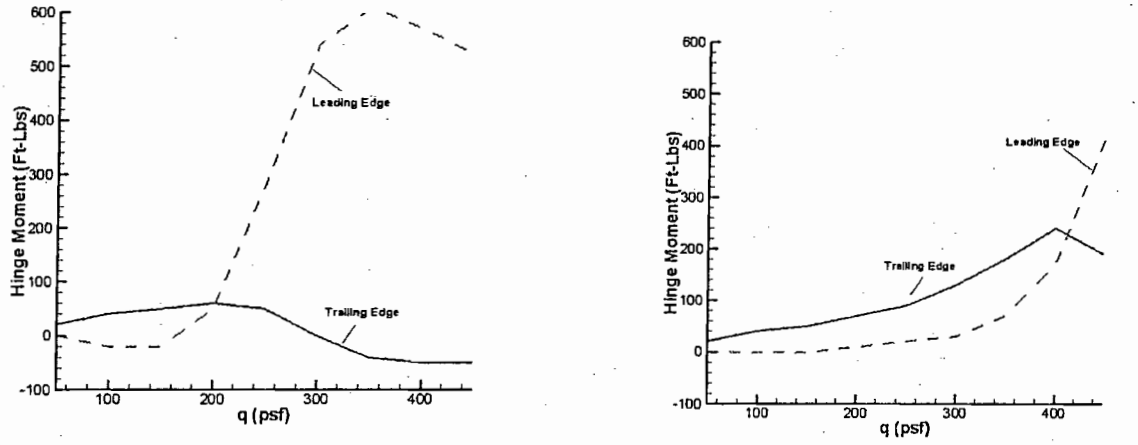

Figure 4 Hinge Moment Distributions for (a) Minimizing Displacement, (b) Minimizing Hinge Moment

Figure 5 shows the distribution of the control surface deflection for the representative UCAV. This is for the case when the objective function is trying to minimize displacement. When one follows the shapes as the dynamic pressure is increasing, the trends are similar in nature to what was seen in the two control surface case discussed above. Figure 6 shows the distribution for the case when the hinge moment is being minimized. It is interesting to note that the leading edge wants to deflect downward in this case, which is a different from the two control surface case. Both cases illustrate that the control surface wants to obtain a range from linear variation to parabolic, which is precisely the capability that the Smart Wing control surface concept. Figures 7 and 8 show the trends in the hinge moment trends for each case. The peak hinge moment for the trailing edge is increased for the case when it is the objective function, but the leading edge hinge moment is dramatically reduced for this case.

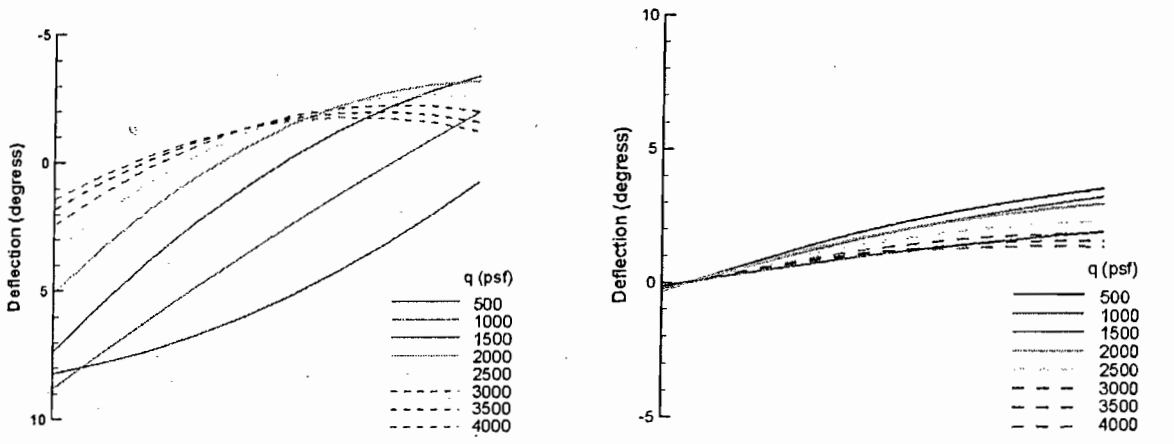

Figure 5 Control Surface Deflections for Minimizing Displacement (a) Trailing Edge, (b) Leading Edge

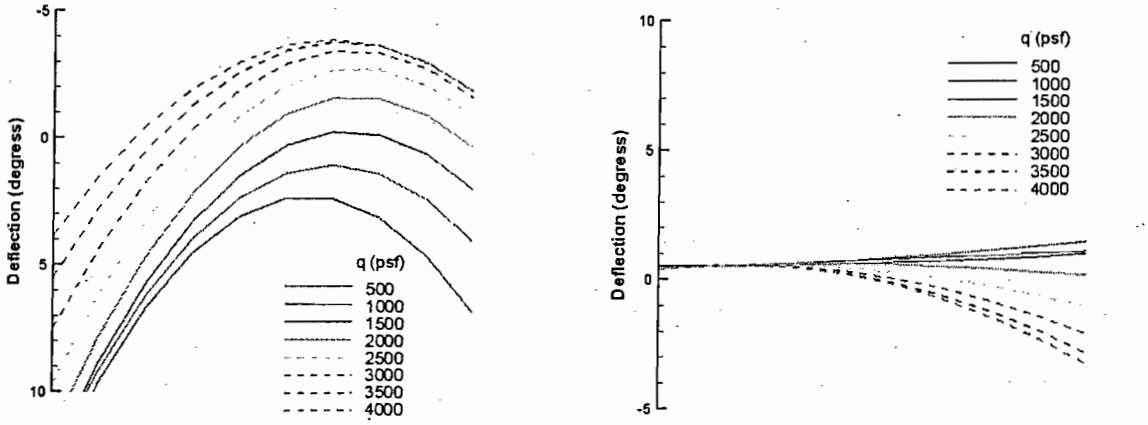

Figure 6 Control Surface Deflections for Minimizing Hinge Moment (a) Trailing Edge, (b) Leading Edge

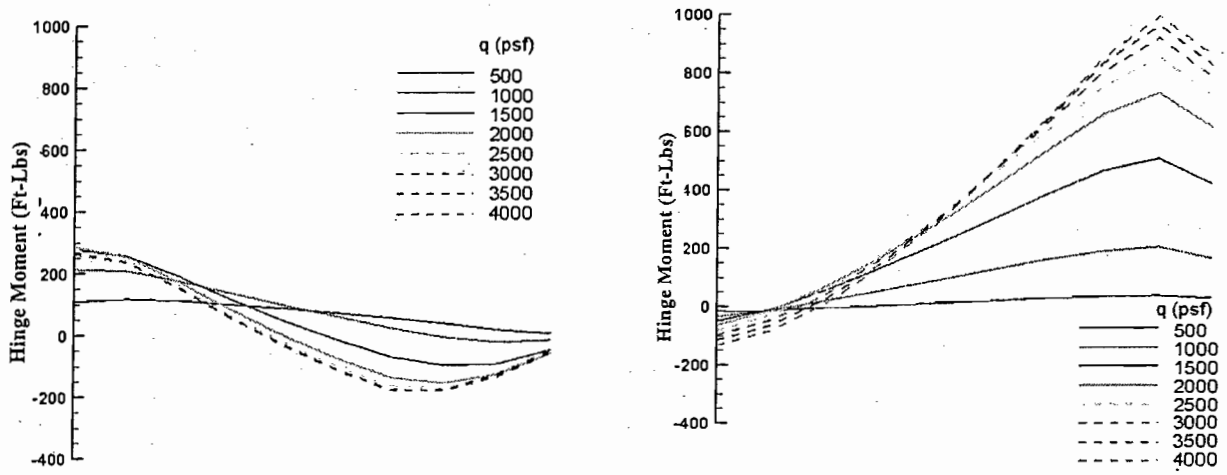

Figure 7 Hinge Moment Distributions for Minimizing Displacement, (a) Trailing Edge, (b) Leading Edge

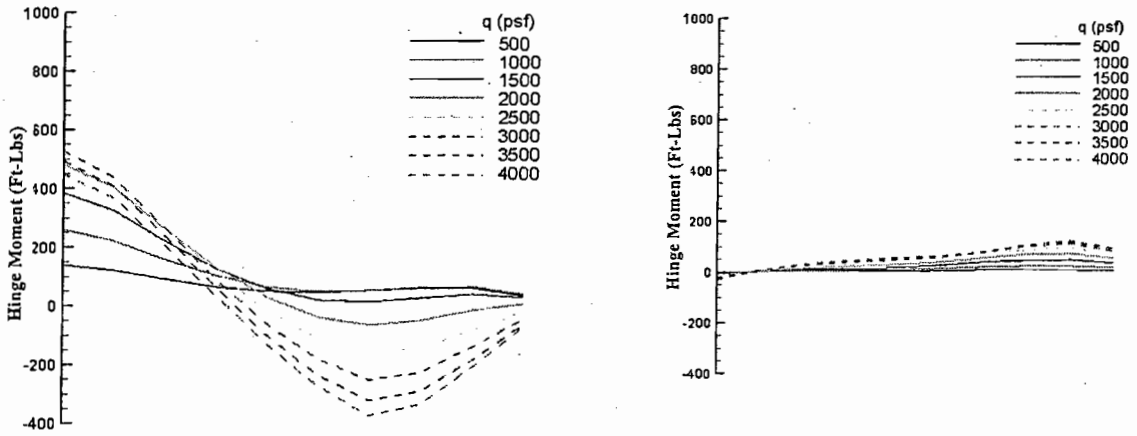

Figure 8 Hinge Moment Distributions for Minimizing Hinge Moment, (a) Trailing Edge, (b) Leading Edge

Drag Performance

Figure 9 shows the typical lift distribution obtained for the UCAV dash condition. The solid line represents the theoretical elliptic distribution while the dashed line shows that obtained for the flexible wing by a coordinated deflection of the control surfaces. It can be observed that the distribution on the wing (e.g., greater that 6 feet) is nearly elliptical. Also, this distribution is obtained for most of the fuselage area. A bad fit occurs in the area where the fuselage and wing join. It is unclear at this point the exact source of this, but future work will include considering control surfaces on the fuselage area. This may be required for other aspects of control too such as pitch and yaw. It should be noted that the angle of attack was considered in the optimization routine, but the large area of the fuselage resulted nearly zero angle of attack in all cases (e.g., dynamic pressure range). Figure 10 shows the control surfaces deflection patterns for this objective function. Again, it is demonstrated that a smooth variation of control surfaces is desired for this case too.

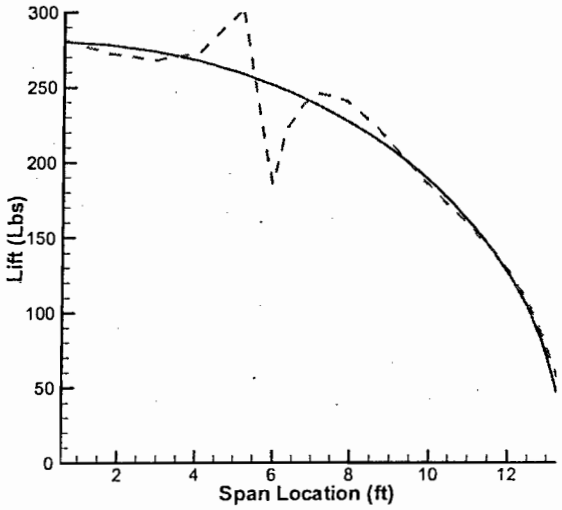

Figure 9 Typical Lift Distribution – rigid wing elliptic – solid line, flexible wing – dashed line

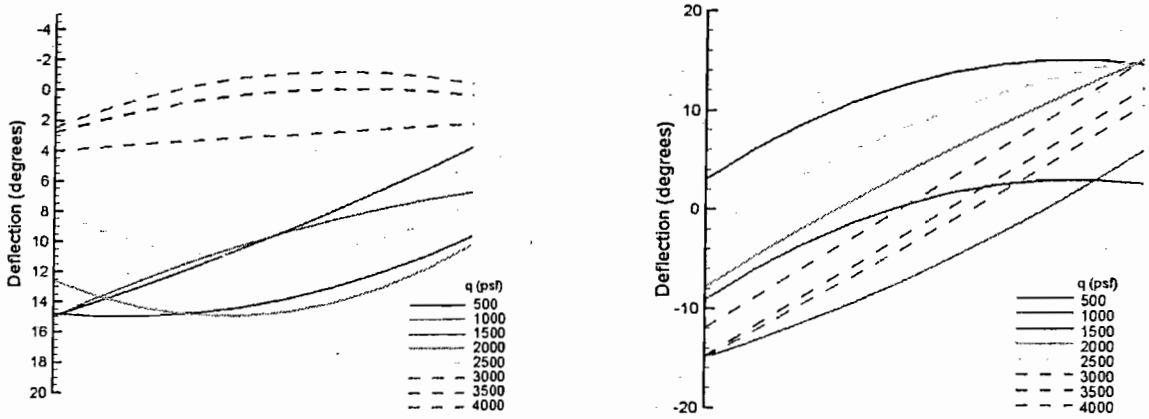

Figure 10 Control Surface Deflections for Minimizing Drag (a) Trailing Edge, (b) Leading Edge

IV. Summary and Future Work

This research investigated the use of smoothly varying, spanwise control surfaces. The work was inspired by the DARPA funded Smart Wing Program. Several optimization formulations where investigated to gain insight into different methods to optimize the hinge moments and vehicle performance. In the long run this is expected to help select and size actuators for the air vehicle system. It was demonstrated that for roll and cruise performance that a large span control surface wants to configure itself into many shapes ranging from a linear variation to a parabolic distribution. Also, it was demonstrated that the control surfaces could control the vehicle well within the deflections achieved during the Smart Wing Program. Further work needs to be explored in the area of understanding pressure distributions and the impact on actuator sizing as a result of the different deflections and hinge moments

V. References

1. Hall, J. M., "Executive Summary AFTI/F-111 Mission Adaptive Wing," Wright Research Development Center, Wright-Patterson Air Force Base, WRDC-TR-89-2083, September 1989.

2. Miller, G.D. 1988, "Active Flexible Wing (AFW) Technology," Air Force Wright Aeronautical Laboratory, TR-87-3096, Wright-Patterson AFB, OH.

3. Kudva, J.,N., "Overview of the DARPA/AFRL/NASA Smart Wing Project", Journal of Intelligent Material Systems and Structures, Vol 15 No 4, April 2004

4. Johnson, E. H., and Venkayya, V. B., "Automated Structural Optimization System (ASTROS) – Vol. 1: Theoretical Manual," AFWAL TR-88-3028, Air Force Wright Aeronautical Laboratory, Wright-Patterson Air Force Base, 1988.

5. Anderson, G., Forster, E., Kolonay, R., and Eastep, F., "Multiple Control Surface Utilization in Active Aeroelastic Wing Technology", J. of Aircraft, Vol 34, No 4., July-August 1997